



Three-dimensional patterning and morphological control of porous nanomaterials by gray-scale direct imprinting

Judson D. Ryckman, Yang Jiao & Sharon M. Weiss

Department of Electrical Engineering and Computer Science, Vanderbilt University, Nashville, TN 37235, USA.

SUBJECT AREAS:
STRUCTURAL PROPERTIES
NANOPORES
OPTICAL MATERIALS AND
STRUCTURES
SURFACE PATTERNING

Received
5 December 2012

Accepted
5 March 2013

Published
21 March 2013

Correspondence and
requests for materials
should be addressed to
S.M.W. (sharon.
weiss@vanderbilt.edu)

We present a method for direct three-dimensional (3D) patterning of porous nanomaterials through the application of a premastered and reusable gray-scale stamp. Four classes of 3D nanostructures are demonstrated for the first time in porous media: gradient profiles, digital patterns, curves and lens shapes, and sharp features including v-grooves, nano-pits, and ‘cookie-cutter’ particles. Further, we demonstrate this technique enables morphological tuning and direct tailoring of nanomaterial properties, including porosity, average pore size, dielectric constant, and plasmonic response. This work opens a rapid and low-cost route for fabricating novel nanostructures and devices utilizing porous nanomaterials, with promising applications spanning diffractive and plasmonic sensing, holography, micro- and transformation optics, and drug delivery and imaging.

Three-dimensional (3D) surface patterning technologies enable complex micro- and nano-structures to be realized that are otherwise unachievable by conventional two-dimensional (2D) patterning routes. Gray-scale lithography (GSL) is one category of 3D surface patterning wherein both lateral and vertical dimensions can be precisely and arbitrarily tailored at the surface of a chip. Primary examples of GSL include gray-scale variants of electron-beam lithography (EBL), laser direct write and masked photolithography, and focused ion-beam milling^{1–3}. When applied to materials ranging from semiconductors, to metals and polymers, 3D surface patterning technologies enable applications in diffractive and micro-optics^{4–6}, holography⁷, plasmonics and transformation optics^{8,9}, and micro-electro-mechanics (MEMS)¹⁰. Compared to most bulk and thin-film solids, porous nanomaterials offer a large internal surface area and distinct optical, electrical, and mechanical properties that can be controlled over a wide range by adjusting the pore morphology (i.e. porosity, pore size, and shape). Combined with their self-organizing and often cost-effective production, porous nanomaterials have recently found wide-spread applications in biomaterials^{11,12}, label-free chemical or biological sensing^{13–16}, drug delivery and imaging^{17,18}, and surface enhanced Raman spectroscopy (SERS)¹⁹. Extending GSL techniques to this class of materials is an especially attractive, yet unexplored, combination that would enable their unique nanoscaled properties to be further exploited in a variety of applications. Porous nanomaterials also offer a unique opportunity to arbitrarily manipulate the internal porous network to yield tailored material properties across the surface of a chip; subwavelength lateral tuning of morphology or effective optical properties is not readily achievable with other material platforms.

Direct imprinting of porous substrates (DIPS) was recently demonstrated as a rapid, low-cost, and high fidelity approach for directly patterning porous nanomaterials²⁰. DIPS overcomes many of the challenges and limitations faced when implementing conventional lithographic strategies on porous substrates. Notably, conventional lithographic strategies and etching techniques are generally expensive, both in terms of time and cost, and are limited by a trade-off between resolution and throughput²¹. While traditional nano-imprint lithography (NIL) is promising for overcoming this tradeoff, NIL and other lithographic methods involve the use of an intermediate resist or thermoplastic, which often must undergo lengthy thermal processing (i.e., curing or baking). DIPS is conceptually similar to room temperature NIL, which can be performed to directly pattern functional device layers, at room temperature, using a pre-patterned and reusable stamp²². Both techniques can eliminate the need to perform intermediate masking, exposures, development, or etching steps; however, room temperature NIL is generally applied to organics or resins, while DIPS is specifically motivated for patterning porous substrates.



Importantly, DIPS addresses challenges that may arise when implementing conventional lithographic techniques on porous substrates, such as chemical incompatibilities with developers, poor resist adhesion, infiltration deep into the pores, or irrevocable corroding or clogging of the porous network. DIPS can be performed in less than one-minute at room temperature and achieves a high patterning resolution (<100 nm) primarily limited by the pore size²⁰. To date, DIPS has only been demonstrated using binary patterns, where a 2D stamp pattern is transferred to the porous substrate at a uniform depth across the sample. However, there is no fundamental limitation in extending DIPS to 3D pattern replication by using a premastered 3D stamp. 3D imprinting and molding have been demonstrated in a variety of techniques on solid substrates including replica molding using elastomeric masters²³, step-and-flash imprint lithography using multi-level patterned stamps^{24,25}, nanotransfer printing using conformal ink layers²⁶, and electrochemical nanoimprinting using solid-state superionic stamps²⁷.

In this work, we adapt the DIPS technique to controllably tailor porous nanomaterials, including nanoporous gold (npAu) and mesoporous silicon (pSi), in a 3D fashion. This process, which we refer to as ‘gray-scale direct imprinting of porous substrates’, is shown to enable not just gray-scale surface morphologies, but gray-scale tunable material properties, as well. As a result, gray-scale DIPS enables the rapid and low-cost fabrication of nanostructures and devices that would be impossible to achieve by other 3D or gray-scale lithographic methods.

Results

Figure 1 illustrates the gray-scale DIPS technique. First, a pre-patterned silicon stamp with a gray-scale pattern, for example a blazed diffraction grating, is brought into contact with a porous substrate, which is prepared on a solid substrate support. Imprinting is then performed by applying a pressure on the order of 100 N/mm² (100 MPa), resulting in local densification of the porous network and direct patterning of the porous substrate. No thermal processing is required. The stamp can then be removed and reused many times²⁰. To demonstrate the basic function of gray-scale DIPS, we imprinted a ~ 200 nm high, 10 μ m period blazed grating silicon stamp into a ~ 500 nm thick, high-porosity pSi thin-film with a pressure of ~ 220 N/mm². Atomic force microscopy (AFM) images, shown in Fig. 1, reveal the high fidelity 1:1 pattern transfer of the gray-scale pattern that resulted in a ~ 200 nm height blazed pSi diffraction grating. The realization of such a grating is technologically important for enhancing diffraction efficiency, and could be implemented to improve coupling efficiency in grating-coupled pSi waveguide biosensors or improve the diffraction efficiency in porous diffraction based biosensors^{14,28}. More advanced grating designs could enable porous nanomaterials to be cheaply implemented in a variety of diffractive optics applications, spanning from diffractive-lenses to holography, while offering a wider range of refractive indices compared to most plastics/polymers^{6,7,23}.

The fabrication of a blazed grating, as shown in Fig. 1, illustrates the basic concept of the gray-scale DIPS technique. In general, this process can be applied to realize a much wider variety of 3D patterns while further offering the unique ability to modify morphology and nanomaterial properties. In the following sections, we step through a number of relevant 3D patterns including (i) gradient profiles, (ii) digital patterns, (iii) curvilinear elements and lens shapes, and (iv) sharp features including v-grooves, nano-pits, and ‘cookie-cutter’ particles. As we demonstrate these 3D patterns, we also highlight the morphological control that can be achieved over key nanomaterial properties including pore dimensions, porosity, dielectric constant or refractive index, and plasmonic response. These novel capabilities are further examined in the context of existing technologies and potential device applications.

Gradient profiles and morphologies. Figure 2 shows scanning electron microscope (SEM) and optical microscope images of a ~ 2 μ m thick high porosity pSi film after applying gray-scale DIPS with a ~ 1.5 μ m height contoured silicon grating stamp. By imprinting deep gradient features into a pSi film of microscale thickness, a wide range of tailored properties can simultaneously be patterned and readily examined through standard SEM and optical imaging techniques. Cross-sectional SEM (Fig. 2a,b) reveals a smoothly varying microscale height profile in the patterned pSi layer. Notably, the gray-scale profile is achieved by imparting a gray-scale densification to the porous layer. The reduction in layer thickness is accommodated by a plastic deformation wherein the pores are permanently bent or compressed together, yielding a reducing porosity with increasing imprint depth. SEM reveals that the interior nano-structured porous matrix is continuously restructured, resulting in a gradient of porosities ranging from the initial $\sim 80\%$ high porosity to a very low, nearly 0% , porosity. Throughout most of the pattern, the local nanostructure and porosity appear to be very uniform within vertical slices (z -direction) of the pSi layer. Some buckling of the pores occurs along the lowest portion of the thicker regions in the patterned film, similar to the over-stamping effect noted in our earlier work²⁰. This effect can be enhanced or removed by changing the stamp height relative to the porous layer thickness, or by changing the applied pressure to adjust the imprinted film fraction. The imprinted film fraction is defined as $f = d/L$, where d is the imprint depth and L is the layer thickness. Examining this structure with top view SEM (Fig. 2c) reveals a gradient in the average pore opening size, ranging from approximately 30 nm to <5 nm, which coincides with the gradient in height and porosity observed from cross-sectional imaging. Optical microscopy (Fig. 2d) reveals that this gray-scale patterned pSi film exhibits strong variations in white light reflectivity. The observed color gradients, which span the entire visible spectrum, result from the strongly modulated optical thickness (product of index and thickness, nL) directly affecting the Fabry-Pérot interference of the single layer thin-film. In Figures 2e,f we present calculations that provide a

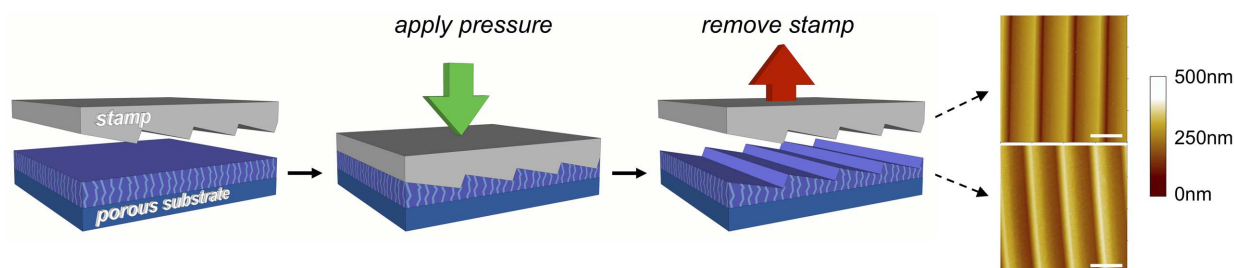


Figure 1 | Illustration of gray-scale direct imprinting of porous substrates. A prepatterned and reusable stamp with a 3D gray-scale profile is imprinted into the porous substrate. The underlying porous nanomaterial is restructured, forming the desired 3D pattern. Example AFM scans of a blazed grating stamp and the subsequently patterned pSi substrate are shown on the right. White scale bars indicate 10 μ m.

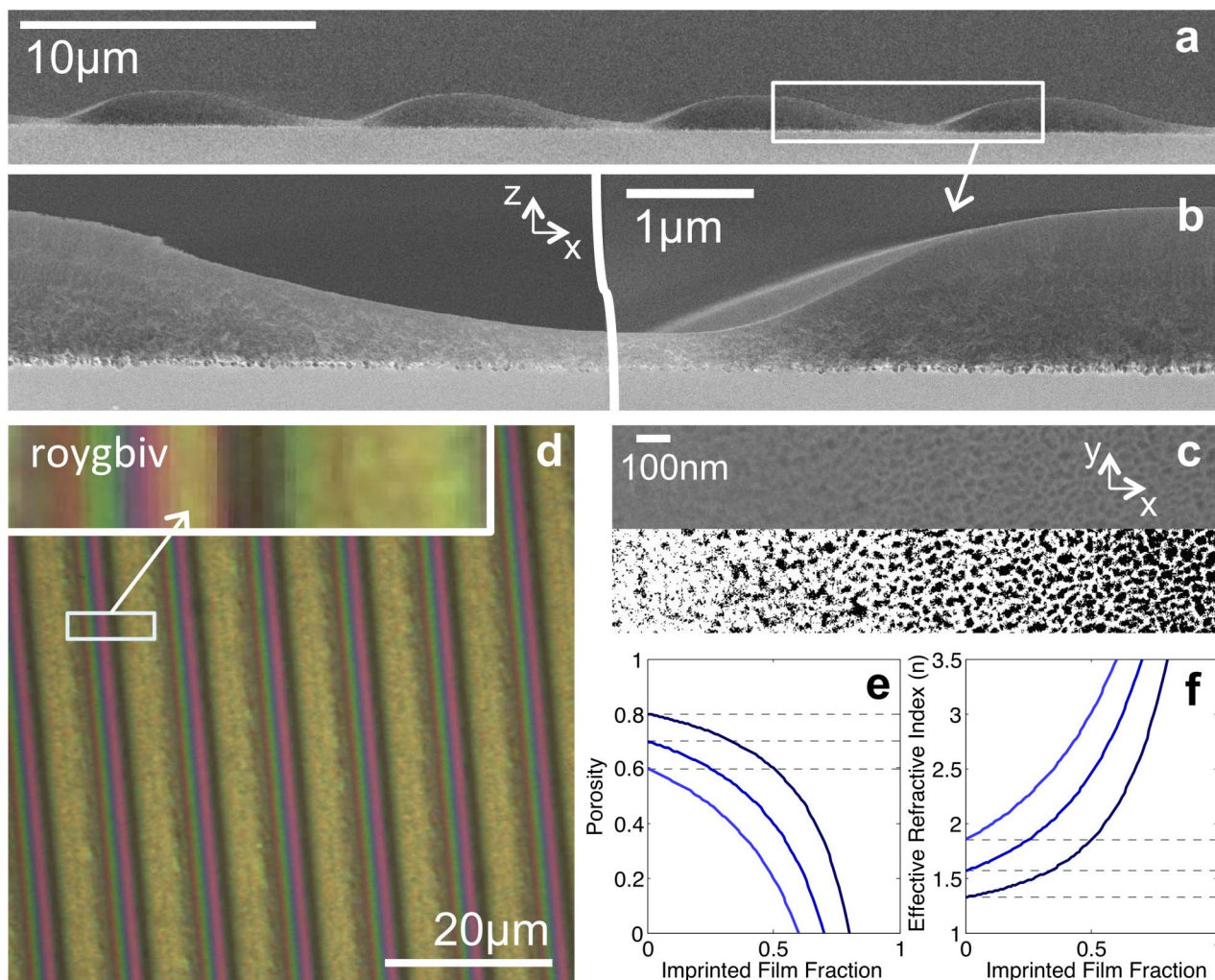


Figure 2 | Patterning height, pore opening size, porosity and refractive index of pSi. (a), (b) Cross sectional SEM images of a gray-scale patterned pSi film with a microscale height profile. (c) Top down SEM image and binary image revealing the gradient patterned pore opening; the estimated pore sizes are tuned from ~ 30 nm to < 5 nm in diameter. (d) Top down optical microscope image of the same pSi film under white-light illumination, revealing a strongly modulated Fabry-Pérot color response. (e) Calculated variation in porosity and (f) refractive index for pSi thin films as a function of imprinted film fraction.

guide illustrating how adjusting the imprint depth tunes film porosity and effective refractive index. These calculations assume uniform densification, achieved solely through a reduction of the void fraction, and an isotropic refractive index determined from a Bruggeman effective medium approximation. Based on these primary assumptions, the maximum imprintable film fraction is therefore equal to the initial porosity. Gray-scale imprinting on a high porosity, low refractive index pSi film would thus enable a wide range of refractive indices, from ~ 1.3 to 3.5, to be realized with almost any arbitrarily designed lateral index gradient. Transfer-matrix calculations (Supporting Information Figure S1) confirm a dramatic blue-shifting color change occurs in response to imprinting.

Combined with well-established etch tuning of out-of-plane parameters (i.e., porosity and refractive index)^{13,15,28,29}, gray-scale DIPS tunes in-plane parameters to provide a new dimension of control, and enables a new class of 3D structures to be realized. The gray-scale DIPS patterned pSi sample shown in Figure 2 demonstrates, for the first time, a method for manipulating the internal porous network and continuously and controllably patterning height, porosity, and pore opening size on the surface of a chip. Such a technology is expected to enable or enhance variety of device capabilities using porous nanomaterials. For example, patterning the pore opening size could be exploited for size-selective filtration or sensing

applications³⁰, where integrating an array of different pore sizes into a compact area, on a single chip, could enable rapid and multiplexed screening of target analytes with a specific size. Patterning the pore dimensions could also be used to spatially modulate or tune transport kinetics through the nanoscale pores³¹. Gray-scale patterning of porosity, meanwhile, could be exploited to locally control the effective refractive index and realize compact gradient index optical structures based on porous nanomaterials.

Morphological control over dielectric constant and plasmonic response. Nanoporous gold (npAu) is a unique, metallic porous nanomaterial which can support both propagating and localized surface plasmonic effects^{32–35}. Each of these effects are particularly sensitive to the effective dielectric constant and pore dimensions, respectively. Controlling the pore dimensions and porosity of npAu is typically achieved during fabrication by adjusting the dealloying parameters³⁶, or by post process annealing or electroplating steps^{37,38}. To our knowledge, no method has ever demonstrated tunable and localized patterning of the pore size, porosity, or dielectric function in a planar metallic film.

Figures 3a,b reveal the complex dielectric function of npAu, as determined by ellipsometry, after uniformly imprinting npAu films to depths ranging from 0–68 nm. Compared to bulk gold, as



prepared npAu features a less negative real part of the dielectric constant, owing to its heterogeneous composition and reduced “metallic-like” character. After imprinting, however, the porosity is reduced and the real part of the dielectric constant is significantly decreased, *i.e.*, from $\text{Re}(\epsilon_r) = -4.15$ to $\text{Re}(\epsilon_r) = -9.72$ at $\lambda = 800$ nm. Imprinting similarly tunes the imaginary part of the dielectric constant, $\text{Im}(\epsilon_r)$, to approach that found for bulk Au. Consistent with other reports for as prepared npAu, $\text{Im}(\epsilon_r)$ is generally 2–3 times smaller than for bulk Au in the ultra-violet and near-infrared regions, while $\text{Im}(\epsilon_r)$ is up to twice as large compared to bulk Au at visible wavelengths³⁵. We note that the observed changes in dielectric constant do not follow a direct linear relationship with imprint depth. Instead, the dielectric constant is increasingly modified at deeper imprint depths, which is expected given that porosity is also increasingly modified as shown in Fig. 2e. The experimentally measured dielectric constants (Fig. 3a) suggest that the 0–68 nm imprint depths reduce the porosity from $\sim 72\%$ to $\sim 54\%$ after applying a volume average effective medium approximation. As shown in the Supporting Information (Fig. S2), these values are in good agreement with the expected trend for porosity vs. imprinted film fraction. These results confirm that gray-scale DIPS can be used to arbitrarily tune porosity and dielectric constant over a wide range by simply adjusting the imprint depth. This new capability for locally tuning the dielectric constant could be used, for example, to locally control the dispersion of propagating plasmons on npAu and enable the straightforward fabrication of plasmonic meta-devices^{35,39}.

In addition to tailoring the effective dielectric constant, gray-scale tuning of the pore size of npAu also directly affects the activation of localized surface plasmons (LSP) arising from the nanoscaled morphology of npAu^{38,40}. To demonstrate this capability, we used gray-scale DIPS to pattern a 200 μm long gradient height profile in npAu, and used surface enhanced Raman spectroscopy (SERS) to probe for localized electric field enhancements arising from LSP (Fig. 3c). Because gold itself is not Raman active, we attached a monolayer of benzenethiol which has a well-known Raman spectrum and is commonly used as a test molecule for SERS substrates¹⁹. Profilometry was performed to estimate a maximum imprint depth of ~ 75 nm. The gradient densification is readily observed by optical

microscopy in the form of a strong color gradient from dark to light (Fig. 3c). SERS spectra were recorded in a line-scan mapping (red arrow) along the entire 200 μm gradient pattern. The non-imprinted region of the pattern ($d = 0$ nm), where the pore size is the largest, shows no detectable SERS signal (Fig. 3d). As npAu is densified however, a clear enhancement of the SERS signal is observed for all the spectral bands of benzenethiol up to an imprint depth, $d \sim 50$ nm. The broadband SERS enhancement is indicative of the broadband localized plasmon resonance in npAu⁴⁰, and we attribute the observed SERS enhancement to LSP activation and an increasing localized field enhancement with reducing pore size^{37,38,40}. From prior work, the maximum SERS enhancement factor is conservatively estimated to be at least 10^6 and at least one order of magnitude greater than as-prepared npAu¹⁹. Beyond ~ 50 nm imprint depth, the SERS signal is slightly reduced, although it remains detectable. The reduction in SERS enhancement beyond ~ 50 nm imprint depth, is likely due to the average pore size reducing to the point where many of the pores have become closed. If it were possible to continue imprinting until all of the pores were closed, we expect that the SERS signal would disappear entirely, resembling planar Au films. This particular experiment demonstrates that gray-scale DIPS enables not only the patterning of pore size, but also the tailoring of a material’s plasmonic response and resulting SERS enhancement.

Digital patterns. In Figure 4 we demonstrate porous nanomaterials patterned using gray-scale DIPS with three additional types of stamp patterns: (1) digital structures, (2) curvilinear dome shapes, and (3) sharp edges and tips. Digital patterns are formed by creating a stamp with multiple discrete height values, such as the Mario test pattern shown in Figure 4a. This particular pattern is encoded with four different height values, representative of the different colors contained in the Mario source image. Imprinting into a ~ 1.5 μm pSi film enables direct digital patterning of the pSi substrate. Optical microscopy, under white-light illumination (Fig. 4f), reveals a multi-colored image that results from digitizing both the height and refractive index of the pSi layer. A cross-sectional AFM scan (Fig. 4k), taken vertically across the center of the pattern, confirms high-fidelity patterning of four discrete height values in the porous

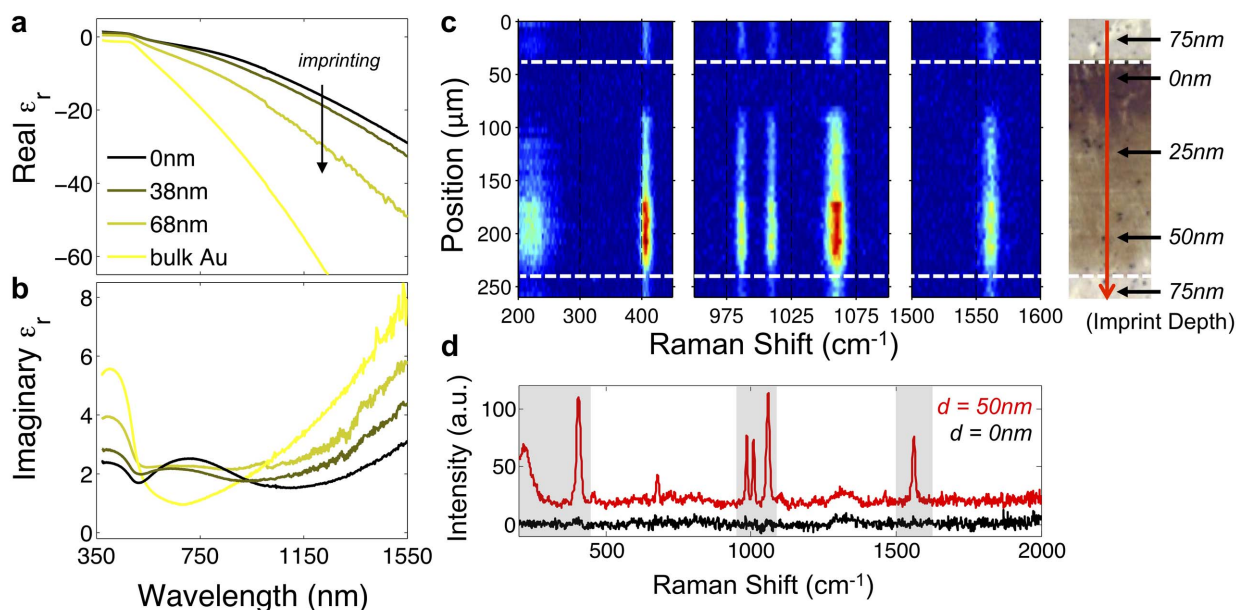


Figure 3 | Tuning dielectric constant and plasmonic SERS enhancement of npAu. (a) The real part and (b) imaginary part of the dielectric constant of npAu, initially ~ 120 nm thick, imprinted at different depths. (c) Line scanned SERS mapping of benzenethiol on gradient densified npAu. The 200 μm long gradient pattern, shown in the rightmost optical microscope image, varies in imprint depth from 0 nm to 75 nm. (d) Full SERS spectrum for benzenethiol on npAu at selected imprint depths, $d = 0$ nm and 50 nm.

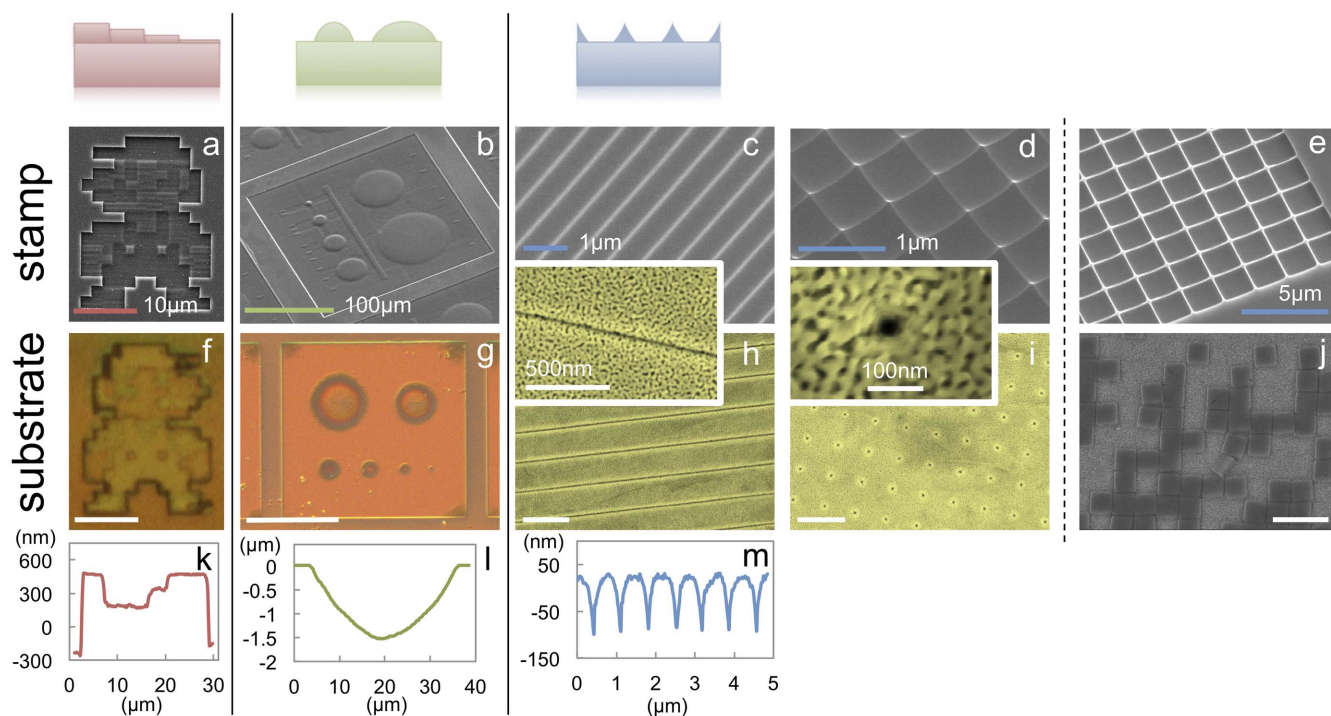


Figure 4 | 3D surface patterning of discrete, curved, and sharp features. Top row (a–e) SEM images of the silicon stamps used to pattern the corresponding porous nanomaterials shown in rows two and three. (f, k) Optical microscope images and AFM line scans of the digitally patterned pSi Mario, and (g, l) gradient index bowl/lens shapes realized in pSi, respectively. (h) SEM images of v-grooves and (i) nano-pits realized in npAu, and (m) the corresponding AFM height profile. (j) SEM image of monodisperse ‘cookie-cutter’ pSi microparticles (dimensions $2 \times 2 \times 0.5 \mu\text{m}$), fabricated with $> 90\%$ packing density and shown loosely adhered to the original substrate. Note: substrate scale bars match their respective stamp images.

substrate. A full AFM mapping of this structure, and subsequent examples, can be found in the Supporting Information (Figure S3). Based on this height profile, our calculations (Fig. 2f) indicate that the porosity and refractive indices have been digitized to values: $\sim 80\%$, 78%, 75%, 62% and ~ 1.32 , 1.37, 1.43, 1.78, respectively. This example suggests that gray-scale DIPS could be used to realize a wide variety of digital patterns in porous nanomaterials, which is especially attractive for holographic applications where arbitrary refractive index tailoring is required to increase the number of phase levels that can simultaneously be achieved. Recent hologram designs utilize lithographic approaches to artificially tailor the refractive index through either an effective medium⁴¹, or metamaterial approach⁴², but are limited in the number of achievable values or the operational wavelength range, respectively, by the patterning resolution. Gray-scale imprinting of porous nanomaterials, on the other hand, provides a route toward locally controlling the effective refractive index solely by the imprint depth. This promotes a broad range of accessible refractive indices while not being limited in the number of achievable index values by the lateral patterning resolution.

Curvilinear elements and lens shapes. Figure 4b shows tilt view SEM of a silicon stamp patterned with dome shaped, 3D curved, structures. Performing gray-scale DIPS with such a stamp enables the replication of bowl shaped gradient index structures in pSi. The gradient optical thickness and smoothly curved pSi profile are readily observable under optical microscopy (Fig. 4g) and AFM (Fig. 4l). Based on AFM measurements and an initial $\sim 2 \mu\text{m}$ film thickness, our calculations (Fig. 2f) indicate that this particular structure contains porosities and refractive indices which smoothly vary from $\sim 80\%$ to 17% and ~ 1.32 to 3.1, respectively. The low-cost fabrication of devices with well-defined optical properties and 3D curvature is technologically important for realizing novel micro-optic devices. We note that it would be possible to utilize

gradient index pSi waveguides to rapidly and cheaply construct in-plane transformation optic devices such as multi-functional meta-devices and optical cloaks^{43–45}. Straightforward calculations (see Supporting Information Figure S4) confirm that imprinting can be used to arbitrarily tune the effective modal index of a pSi waveguide.

Fabrication of nano-grooves and nano-pits. The low-cost fabrication of nanoscaled metallic features, such as tips, grooves, or pits, is desirable for enabling applications spanning plasmonics, SERS, and label-free sensing. Thus, we investigate the application of gray-scale DIPS using a stamp containing sharp edge and tip patterns. SEM images of the fabricated stamps are shown in Figs. 4c–e. Unlike stamps discussed previously, these sharply pointed stamps are fabricated by conventional EBL followed by isotropic reactive-ion etching (RIE). Imprinting into a $\sim 160 \text{ nm}$ thick npAu film enables the replication of sharp 1D v-groove and 2D nano-pit arrays, as shown in Figs. 4h,i. Notably, these patterns represent the smallest features ever patterned into npAu. AFM reveals that the v-grooves and pits are $\sim 109 \text{ nm}$ deep (Fig. 4m). The imprinted film fraction, ~ 0.68 , is comparable to the initial porosity (estimated by a volume average effective medium approximation to be $\sim 72\%$), indicating that npAu can be locally densified into a nearly non-porous state. The ability to pattern sharp nanoscaled features, with $< 100 \text{ nm}$ resolution, combined with the ability to dramatically and locally tune the effective dielectric function (Fig. 3a,b), enables the plasmonic properties of npAu to be tailored with improved freedom^{46,47}. Furthermore, as a direct-to-device technique, gray-scale DIPS enables these nanoscaled features to be replicated without the need for repeated lithography or etching steps.

Fabrication of well defined ‘cookie-cutter’ microparticles. In Figs. 4e,j we show that performing gray-scale DIPS with a sharp-edged stamp pattern enables ‘cookie-cutter’ pSi microparticles to be fabricated. In this example, the $\sim 80\%$ porosity pSi substrate is $\sim 500 \text{ nm}$ thick,



resulting in pSi microparticles precisely tailored in size (e.g., $2 \times 2 \times 0.5 \mu\text{m}$). These high porosity particles are relatively weakly attached to the underlying substrate and many are visibly removed with the stamp after imprinting. The remaining particles can be removed using an adhesive, an electrochemical lift-off step, or by brief sonication in liquid. Notably, with this particular stamp design, we demonstrate that $> 90\%$ areal packing density of highly monodisperse pSi microparticles can be achieved in a single step process. Such particles are particularly attractive for drug delivery and imaging applications^{17,18}. More advanced stamp designs could be used to tailor not only the size and shape of the particles, but also pattern the pore opening size or porosity within a given particle, enabling their optical and mechanical properties or drug loading and release kinetics to be altered.

Discussion

In summary, we have demonstrated the ability to three-dimensionally pattern porous nanomaterials through a rapid and low-cost imprinting technique. Four classes of 3D structures are demonstrated: continuous sloped profiles, digital patterns, curves and lens shapes, and sharp features including v-grooves, nano-pits, and ‘cookie-cutter’ particles. Importantly, beyond patterning 3D geometries, gray-scale DIPS enables nanomaterial properties to be arbitrarily tailored including porosity, average pore size, dielectric constant, and plasmonic response. Gray-scale DIPS thus opens the possibility to construct a new class of structures and devices utilizing porous nanomaterials with promising applications spanning diffractive and plasmonic sensing, holography, micro- and transformation optics, and drug delivery and imaging.

Methods

Porous substrates. pSi films were prepared by electrochemically etching p-type Si(100) wafers ($0.01\text{--}0.02 \Omega\text{cm}$) in a 3 : 7 (v/v) mixture of 49% hydrofluoric acid (HF) and ethanol. Etching was performed at a current density of 80 mA cm^{-2} with the time adjusted to control the film thickness. Reflectance measurements and optical modeling were used to approximate the initial pSi porosity at $\sim 80\%$. The underlying $\sim 475\text{--}550 \mu\text{m}$ thick Si wafer supported the pSi films. npAu films were prepared by a method described in a previous work¹⁸. Briefly, $\sim 1.5 \times 1.5 \text{ cm}$ sheets of $\sim 120\text{--}160 \text{ nm}$ thick Monarch 12 karat white gold (fineartstore.com) are dealloyed by floating on concentrated nitric acid for 15 min. npAu films are mounted on $\sim 475\text{--}550 \mu\text{m}$ thick Si wafers coated with a $> 100 \text{ nm}$ layer of Au, which is surface-modified with 1,6-hexanedithiol for robust anchoring.

Stamps and imprinting. Silicon stamps were prepared from $\sim 475\text{--}550 \mu\text{m}$ thick Si(100) wafers by gray-scale EBL followed by anisotropic RIE, unless otherwise noted. Two different PMMA resists, 950 k A4 (spun at 6,000 rpm and baked at 180°C for 10 min) and 50 k A20 (spun at 2,000 rpm and baked at 180°C for 5 min) are employed to realize either shallow ($\sim 200 \text{ nm}$) or deep ($\sim 1.5 \mu\text{m}$) structures, respectively. Gray-scale EBL (JEOL JBX-9300-100 kV) is performed with a 2 nA beam current, pattern shot pitch of 5 nm, and a base dose of $375 \mu\text{C cm}^{-2}$, with the relative dose modulated from -33% to 0% . Development is performed in a 1 : 2 (v/v) mixture of de-ionized water and IPA for 30 s, followed immediately by drying under nitrogen. Thermal reflow of the resist was performed in some cases to smooth the resist profile and remove roughness by baking at 115°C for 10 min to 1 hr, with intermittent evaluation under dark-field optical microscopy¹⁹. Anisotropic reactive-ion etching was then performed (Oxford PlasmaLab 100) using $\text{C}_4\text{F}_8/\text{SF}_6/\text{Ar}$ process gases to transfer the resist pattern into the Si substrate. For sharply pointed stamps, conventional EBL and isotropic etching in SF_6 were employed. The duration of the isotropic etch is tuned to achieve sharp features at the intersection of neighboring etch fronts. Imprinting was performed in accordance to our prior work²⁰. Briefly, we use a Tinius Olsen Super L 60 k universal testing machine to press a flat metallic plate onto the backside of the stamp, which is covered with single-sided Scotch tape. A computer-monitored force was then delivered and sustained for less than 1 s.

SERS mapping. The gradient patterned npAu sample was immersed in 10 mM benzenethiol in ethanol for 1 hour to attach a monolayer of benzenethiol to the internal gold surface. The sample was then rinsed thoroughly with ethanol and dried under nitrogen flow. SERS measurements were performed using a DXR Raman microscope (Thermo Scientific) with a 780 nm diode laser at 0.9 mW power. A $10\times$ objective ($N = 0.25$) was employed, resulting in a $\sim 3.1 \mu\text{m}$ spot size. Raman spectra were collected in a line-scanning mode with a $5 \mu\text{m}$ step-size, 1 s integration time and averaging of 2 scans.

1. del Campo, A. & Arzt, E. Fabrication approaches for generating complex micro- and nanopatterns on polymeric surfaces. *Chem Rev* **108**, 911–945 (2008).

2. Geissler, M. & Xia, Y. Patterning: Principles and Some New Developments. *Adv Mater* **16**, 1249–1269 (2004).
3. Guo, C. *et al.* Grayscale photomask fabricated by laser direct writing in metallic nano-films. *Opt. Express* **17**, 19981–19987 (2009).
4. Fu, Y. Q., Bryan, N. K. A. & Shing, O. N. Diffractive optical elements with continuous relief fabricated by focused ion beam for monomode fiber coupling. *Opt. Express* **7**, 141–147 (2000).
5. Yu, W. X. & Yuan, X. C. Fabrication of refractive microlens in hybrid $\text{SiO}_2/\text{TiO}_2$ sol-gel glass by electron beam lithography. *Opt. Express* **11**, 899–903 (2003).
6. Levy, U. *et al.* Design, fabrication, and characterization of circular Dammann gratings based on grayscale lithography. *Opt. Lett.* **35**, 880–882 (2010).
7. Urquhart, K. S., Stein, R. & Lee, S. H. Computer-Generated Holograms Fabricated by Direct Write of Positive Electron-Beam Resist. *Opt. Lett.* **18**, 308–310 (1993).
8. Yang, J. C. *et al.* Enhanced Optical Transmission Mediated by Localized Plasmons in Anisotropic, Three-Dimensional Nanohole Arrays. *Nano Lett.* **10**, 3173–3178 (2010).
9. Zentgraf, T., Liu, Y., Mikkelsen, M. H., Valentine, J. & Zhang, X. Plasmonic Luneburg and Eaton lenses. *Nat. Nanotechnol.* **6**, 151–155 (2011).
10. Waits, C., A. M. & Ghodssi, R. Investigation of gray-scale technology for large area 3D silicon MEMS structures. *Journal of Micromechanics and Microengineering* **13**, 170–177 (2003).
11. Sun, W., Puzas, J. E., Sheu, T. J., Liu, X. & Fauchet, P. M. Nano- to microscale porous silicon as a cell interface for bone-tissue engineering. *Adv Mater* **19**, 921 (2007).
12. Low, S. P., Williams, K. A., Canham, L. T. & Voelcker, N. H. Evaluation of mammalian cell adhesion on surface-modified porous silicon. *Biomaterials* **27**, 4538–4546 (2006).
13. Wei, X. *et al.* Grating couplers on porous silicon planar waveguides for sensing applications. *J. Appl. Phys.* **104**, 3113 (2008).
14. Ryckman, J. D., Liscidini, M., Sipe, J. E. & Weiss, S. M. Porous silicon structures for low-cost diffraction-based biosensing. *Appl. Phys. Lett.* **96**, 1103 (2010).
15. Cunin, F. *et al.* Biomolecular screening with encoded porous-silicon photonic crystals. *Nat. Mater.* **1**, 39–41 (2002).
16. Ruffato, G., Romanato, F., Garoli, D. & Cattarin, S. Nanoporous gold plasmonic structures for sensing applications. *Opt. Express* **19**, 13164–13170 (2011).
17. Tasciotti, E. *et al.* Mesoporous silicon particles as a multistage delivery system for imaging and therapeutic applications. *Nat. Nanotechnol.* **3**, 151–157 (2008).
18. Park, J. H. *et al.* Biodegradable luminescent porous silicon nanoparticles for in vivo applications. *Nat. Mater.* **8**, 331–336 (2009).
19. Jiao, Y. *et al.* Patterned nanoporous gold as an effective SERS template. *Nanotechnology* **22**, 5302 (2011).
20. Ryckman, J. D., Liscidini, M., Sipe, J. E. & Weiss, S. M. Direct Imprinting of Porous Substrates: A Rapid and Low-Cost Approach for Patterning Porous Nanomaterials. *Nano Lett.* **11**, 1857–1862 (2011).
21. Sirbuly, D. J., Lowman, G. M., Scott, B., Stucky, G. D. & Buratto, S. K. Patterned microstructures of porous silicon by dry-removal soft lithography. *Adv Mater* **15**, 149 (2003).
22. Khang, D. Y., Yoon, H. & Lee, H. H. Room-Temperature Imprint Lithography. *Adv Mater* **13**, 749–752 (2001).
23. Xia, Y. N. *et al.* Complex optical surfaces formed by replica molding against elastomeric masters. *Science* **273**, 347–349 (1996).
24. Gates, B. D. *et al.* New approaches to nanofabrication: Molding, printing, and other techniques. *Chem Rev* **105**, 1171–1196 (2005).
25. Guo, L. J. Nanoimprint Lithography: Methods and Material Requirements. *Adv Mater* **19**, 495–513 (2007).
26. Zaumseil, J. *et al.* Three-dimensional and multilayer nanostructures formed by nanotransfer printing. *Nano Lett.* **3**, 1223–1227 (2003).
27. Hsu, K. H., Schultz, P. L., Ferreira, P. M. & Fang, N. X. Electrochemical nanoimprinting with solid-state superionic stamps. *Nano Lett.* **7**, 446–451 (2007).
28. Wei, X. & Weiss, S. M. Guided mode biosensor based on grating coupled porous silicon waveguide. *Opt. Express* **19**, 11330–11339 (2011).
29. Jane, A., Dronov, R., Hodges, A. & Voelcker, N. H. Porous silicon biosensors on the advance. *Trends Biotechnol* **27**, 230–239 (2009).
30. Lawrie, J. L., Jiao, Y. & Weiss, S. M. Size-Dependent Infiltration and Optical Detection of Nucleic Acids in Nanoscale Pores. *IEEE Trans. Nanotechnol.* **9**, 596–602 (2010).
31. Velasco, A. E., Friedman, S. G., Pevarnik, M., Siwy, Z. S. & Taborek, P. Pressure-driven flow through a single nanopore. *Phys Rev E* **86**, 025302 (2012).
32. Lang, X. Y., Qian, L. H., Guan, P. F., Zi, J. & Chen, M. W. Localized surface plasmon resonance of nanoporous gold. *Appl. Phys. Lett.* **98**, 093701 (2011).
33. Bok, H. M., Shuford, K. L., Kim, S., Kim, S. K. & Park, S. Multiple surface plasmon modes for a colloidal solution of nanoporous gold nanorods and their comparison to smooth gold nanorods. *Nano Lett.* **8**, 2265–2270 (2008).
34. Yu, F. *et al.* Simultaneous excitation of propagating and localized surface plasmon resonance in nanoporous gold membranes. *Anal Chem* **78**, 7346–7350 (2006).
35. Sardana, N., Heyroth, F. & Schilling, J. Propagating surface plasmons on nanoporous gold. *J Opt Soc Am B* **29**, 1778–1783 (2012).



36. Ding, Y., Kim, Y. J. & Erlebacher, J. Nanoporous gold leaf: "Ancient technology"/ advanced material. *Adv Mater* **16**, 1897–1900 (2004).
37. Qian, L. H., Yan, X. Q., Fujita, T., Inoue, A. & Chen, M. W. Surface enhanced Raman scattering of nanoporous gold: Smaller pore sizes stronger enhancements. *Appl. Phys. Lett.* **90**, 153120 (2007).
38. Lang, X. Y., Chen, L. Y., Guan, P. F., Fujita, T. & Chen, M. W. Geometric effect on surface enhanced Raman scattering of nanoporous gold: Improving Raman scattering by tailoring ligament and nanopore ratios. *Appl. Phys. Lett.* **94**, 213109 (2009).
39. Zheludev, N. I. & Kivshar, Y. S. From metamaterials to metadevices. *Nat Mater* **11**, 917–924 (2012).
40. Bosman, M., Anstis, G. R., Keast, V. J., Clarke, J. D. & Cortie, M. B. Light Splitting in Nanoporous Gold and Silver. *ACS Nano* **6**, 319–326 (2012).
41. Freese, W., Kämpfe, T., Kley, E.-B. & Tünnermann, A. Design of binary subwavelength multiphase level computer generated holograms. *Opt. Lett.* **35**, 676–678 (2010).
42. Larouche, S., Tsai, Y.-J., Tyler, T., Jokerst, N. & Smith, D. Infrared metamaterial phase holograms. *Nat. Mater.* **11**, 450–454 (2012).
43. Gharghi, M. *et al.* A Carpet Cloak for Visible Light. *Nano Lett.* **11**, 2825–2828 (2011).
44. Valentine, J., Li, J., Zentgraf, T., Bartal, G. & Zhang, X. An optical cloak made of dielectrics. *Nat. Mater.* **8**, 568–571 (2009).
45. Zentgraf, T., Valentine, J., Tapia, N., Li, J. & Zhang, X. An Optical "Janus" Device for Integrated Photonics. *Adv Mater* **22**, 2561–2564 (2010).
46. Sondergaard, T. *et al.* Plasmonic black gold by adiabatic nanofocusing and absorption of light in ultra-sharp convex grooves. *Nat. Commun.* **3**, 969 (2012).
47. Lee, S., Shin, J., Lee, Y. H. & Park, J. K. Fabrication of the Funnel-Shaped Three-Dimensional Plasmonic Tip Arrays by Directional Photofluidization Lithography. *ACS Nano* **4**, 7175–7184 (2010).
48. Ciesielski, P. N. *et al.* Functionalized Nanoporous Gold Leaf Electrode Films for the Immobilization of Photosystem I. *ACS Nano* **2**, 2465–2472 (2008).
49. Schleunitz, A., Guzenko, V. A., Schander, A., Vogler, M. & Schiff, H. Selective profile transformation of electron-beam exposed multilevel resist structures based on a molecular weight dependent thermal reflow. *J Vac Sci Technol B* **29**, F302 (2011).

Acknowledgments

This work was supported in part by the Army Research Office (W911NF-09-1-0101). A portion of this research was conducted at the Center for Nanophase Materials Sciences, which is sponsored at Oak Ridge National Laboratory by the Scientific User Facilities Division, Office of Basic Energy Sciences, U.S. Department of Energy. Portions of this work were also performed at the Vanderbilt Institute of Nanoscale Science and Engineering, using facilities renovated under NSF ARI-R2 DMR-0963361. The authors thank J. Valentine and J. Garnett for providing the 50 k PMMA resist and for helpful discussions; K. Jennings and C. Escobar for providing npAu; F. Sanchez and L. Brown for assistance with the stamping tool; D. Koktysh for assistance with the Raman microscope; J. Mares for helpful discussions; and I. Kravchenko and S. Retterer for their guidance at CNMS. J.D.R. acknowledges support from an NSF Graduate Research Fellowship.

Author contributions

S.M.W. guided the experiments and project development. J.D.R. conceived, designed, and fabricated the stamps and nanostructures. Y.J. performed the optical and SERS characterization of npAu structures. All authors contributed to experiment analysis and manuscript preparation.

Additional information

Supplementary information accompanies this paper at <http://www.nature.com/scientificreports>

Competing financial interests: The authors declare no competing financial interests.

License: This work is licensed under a Creative Commons Attribution-NonCommercial-NoDerivs 3.0 Unported License. To view a copy of this license, visit <http://creativecommons.org/licenses/by-nc-nd/3.0/>

How to cite this article: Ryckman, J.D., Jiao, Y. & Weiss, S.M. Three-dimensional patterning and morphological control of porous nanomaterials by gray-scale direct imprinting. *Sci. Rep.* **3**, 1502; DOI:10.1038/srep01502 (2013).